Author Manuscript

Author Manuscript

Author Manuscript

Author Manuscript

HHS Public Access

Author manuscript

*Nanotechnology*. Author manuscript; available in PMC 2019 December 14.

Published in final edited form as:

*Nanotechnology*. 2018 December 14; 29(50): 504001. doi:10.1088/1361-6528/aae272.

# A gold nanoparticle system for enhancement of radiotherapy and simultaneous monitoring of reactive-oxygen-species formation

**Jihye Choi**[1,2], **Kyung Oh Jung**[1], **Edward E. Graves**[1], and **Guillem Pratx**[1,*]

[1]Department of Radiation Oncology, Stanford University School of Medicine, Stanford, CA 94305

[2]Severance Biomedical Science Institute, Yonsei University of College of Medicine, Seoul, 03722, Republic of Korea

## Abstract

Gold nanoparticles (AuNPs) are known to sensitize cancer cells to radiation therapy (RT) by increasing the deposition of ionizing energy in their immediate vicinity. However, this process of dose enhancement is challenging to monitor because it is heterogeneous at the sub-cellular scale. Furthermore, radiation damage is primarily mediated by reactive oxygen species (ROS) that are produced following water radiolysis. Here, radiation-responsive PEGylated gold nanoparticles (RPAuNPs) were synthesized for enhanced generation and concurrent detection of ROS in cancer cells and tumors. PEGylated gold particles (20 nm diameter) were functionalized with dihydrorhodamine 123 (DHR-123), a known ROS sensor, to monitor ROS generation in their immediate vicinity. These nanoparticles were able to effectively radiosensitize cells, as measured by increased cell apoptosis following RT. Furthermore, the fluorescence of these RPAuNPs was sevenfold higher after 6 Gy RT due to local production of ROS near the surface of the nanoparticle. Finally, multispectral fluorescence imaging was used to monitor nanoparticle-induced ROS *in vivo*, following conformal RT, in a xenograft model of breast cancer. This theranostic nanoparticle system provides a novel approach for monitoring the nanoscale enhancement of RT by high-Z metal nanoparticles.

### Keywords

optical imaging; gold nanoparticle; reactive oxygen species; radiation therapy

## 1. Introduction

Radiation therapy (RT) is an essential tool for managing cancer, used in over half of all cancer [1]. This therapy deposits ionizing energy (the dose) into tumors, typically by irradiation with X-ray photons, to kill cancer cells or the vasculature that feeds them [2]. The probability of tumor control increases with higher radiation dose, but collateral toxicity to surrounding organs sometimes prevents radiation oncologists from delivering a sufficient

*Corresponding author: Guillem Pratx, 300 Pasteur Dr, Grant S277, Stanford, CA 94305, Ph: +1 (650) 724 – 9829, pratx@stanford.edu.

Author Manuscript Author Manuscript Author Manuscript Author Manuscript

dose to the tumor [3]. While radiation beams can be collimated laterally to avoid damage to normal tissues, significant dose is still received by normal tissues along the beam path. Because of these constraints, there is increasing interest in using tumor-targeted noble-metal nanoparticles (NPs) to physically enhance the radiation dose received by the tumor while limiting dose to the healthy surrounding. Gold nanoparticles (AuNPs) in particular have been extensively studied due to their high density and atomic number (Z=79), well-established synthesis, straightforward functionalization, unique optical properties, and favorable biocompatibility profile [4–8].

Physical radiosensitization of tumors by high-Z nanoparticles is particularly complex due to the multiplicity of physical mechanisms involved. In the kilovoltage range (50–300 kVp), AuNPs greatly enhance local dose deposition due to their high photoelectric absorption crosssection. X-ray photons absorbed by AuNPs through this effect transfer their energy to surrounding molecules via secondary ionizing electrons. Of these, Auger electrons play a particularly important role in radiosensitizing tumors [9, 10]. Upon irradiation, showers of these low-energy electrons (< 5 keV) are emitted from the NP and deposit their energy in the immediate vicinity (<1 μm), resulting in local dose enhancement. In addition, due to their higher rate of linear energy transfer (LET), Auger electrons cause more severe damage to the DNA than more energetic electrons [11, 12].

Given the short range of Auger electrons, it is important to understand that the biological effects of AuNPs are not accurately modeled by conventional dosimetry models, which assume radiation dose to be spatially homogeneous. Instead, one must consider the heterogeneity of the dose distribution at the nanometer scale. Microdosimetric Monte Carlo simulation have shown that dose enhancement is highest near the surface of the AuNP and decreases rapidly away from it [13]. As a result, effective radiosensitization is achieved when the AuNPs are located close to vital cell organelles, such as the nucleus or mitochondria [14]. Another recent study has highlighted the importance of selecting the appropriate physical model to describe energy deposition at the nanoscale level by electrons [15]. In this context, there is strong value in measuring experimentally the radiosensitizing effect of AuNPs at the nanoscale.

Importantly, 70% of radiation-induced DNA damage is indirect [16]. Most of the energy imparted to the AuNP by ionizing radiation is transferred to surrounding water, leading to its radiolysis. The resulting free radicals and reactive oxygen species (ROS) are the primary mediators of DNA damage and cell death. Due to their short diffusion range, the local concentration of radiation-induced ROS parallels the dose distribution at the nanoscale, with the highest concentration of ROS found close to the surface of the AuNP. Efforts to model the chemical and biological effects of AuNPs during cell irradiation have been carried out using various computational models [17, 18], but there is still a lack of suitable experimental methods to confirm these findings. In addition, nanoparticles have potent catalytic effects and may facilitate the radiolysis of water near their surface beyond what would be expected based on energy deposition alone [19]. Nanoparticles have also been designed to enhance water radiolysis by combining the catalytic properties titanium dioxide and the X-ray absorption of gold [20].

Author Manuscript Author Manuscript Author Manuscript Author Manuscript

The local nature of dose enhancement around AuNPs is critical for understanding cell killing and DNA damage [21]. However, while downstream biological effects of AuNP-enhanced RT can be assessed using biological assays, the local increase in dose near the nanoparticle has only been predicted by microdosimetry models and never measured experimentally. Here, we synthesized radiation-responsive PEGylated gold nanoparticles (RPAuNPs) that can report the local ROS concentration enhancement in the vicinity of the NP through functionalization with a fluorescent ROS indicator, dihydrohodamine 123 (DHR-123). This commercial ROS indicator, initially non-fluorescent due to the reduction of its iminium cation, becomes permanently fluorescent after oxidation by ROS. We evaluated the ability of these RPAuNPs to report on ROS generation *in vitro* in cancer cells and assessed the resulting cell killing. We also investigated this effect *in vivo* in a mouse tumor xenograft model of breast cancer. This new nanotechnology platform will be useful for validation and verification of AuNP-enhanced radiation therapy both *in vitro* and *in vivo*.

## 2. Materials and Methods

### Synthesis of PEGylated gold nanoparticles (PAuNPs).

Gold nanoparticles (AuNPs) were synthesized according to the reduction protocol in fresh aqueous Triton X-100 solution [22]. To prepare PEGylated gold nanoparticles (PAuNPs), AuNPs were coated with hetero bi-functionalized PEG as a stabilizer. Fifty milligrams of carboxymethyl-PEG-thiol (CM-PEGSH; MW: 3,400; Laysan Bio) was added to 1 mL of AuNPs solution (300 μg of Au/mL) and then stirred for 24 h at room temperature. The mixture was centrifuged at 12,500 rpm for 15 min to remove unbound PEG molecules and was then re-suspended in 1 mL of DI water.

### Preparation of PEGylated gold nanoparticles radiosensitizing agent (RPAuNPs).

To conjugate dihydrorhodamine 123 (DHR-123) to PAuNPs or CM-PEG-SH (control), 1-ethyl-3(3-dimethylaminopropyl)-carbodiimide (EDC, $8.82\times10^{-2}$ mmol), N-hydrosuccinimide (NHS, $8.82\times10^{-2}$ mmol), and DHR-123 (0.9 μmol/100 μL) were added to 1 mL of either PAuNPs (300 μg of Au/mL) or CM-PEG-SH solution, and reacted at room temperature for 24 h. After the reaction, side-products were removed by centrifugation at 12,500 rpm for 15 minutes and were re-dispersed in 1 mL of PBS.

### Characterization of AuNPs and PAuNPs.

Absorbance of AuNPs and PAuNPs was measured by optical spectrometry (SpectraMax M2e, Molecular Devices, San Jose, CA). The morphology of the NPs was evaluated using high-resolution transmission electron microscopy (HR-TEM, JEM-2100 $LAB_6$, JEOL Ltd., Japan).

### ROS generation and detection by RPAuNPs *in vitro*.

To measure ROS generation *in vitro*, 100 μL of RPAuNPs (7.75 μg/mL) and PEG-DHR123 (5 mg/ 100 μL) were placed in a 96 well microplate. These wells were treated using different doses of X-ray radiation (2, 4, 6, 8 and 10 Gy; 320 kVp) using an X-RAD 320 irradiator (PXi, North Branford, CT). The irradiated samples were then excited at 500 nm and their fluorescence emission at 530 nm was measured using a UV-Vis plate reader (SpectraMax

Author Manuscript Author Manuscript Author Manuscript Author Manuscript

M2e). Relative fluorescence intensity is defined as ΔRFU = ($F$-$F_0$) / $F_0$, where $F$ and $F_0$ are the measured fluorescence intensities with and without exposure to radiation, respectively.

### *In vitro* assessment of cell viability.

Cell viability was quantified using a colorimetric assay based on tetrazolium salt (WST-1; Roche). A human breast adenocarcinoma cell line, MDAMB-231, was obtained from the American Tissue Type Culture (ATCC). Cells were plated at a density of $8\times10^3$ cells/ 100 μL in a 96-well plate and were incubated at 37 °C in 5 % $CO_2$ atmosphere in Dulbecco's Modified Eagle Medium (DMEM) supplemented with 10 % fetal bovine serum (FBS) and 1 % Penicillin streptomycin (PS). The cells were incubated for 24 h with 100 μL of PAuNP or RPAuNP (up to 7.75 μg of Au/mL) re-suspended in 100% media, and then rinsed with 100 μL of phosphate buffered saline (PBS, pH 7.4, 1X). The cells were then added to 100 μL media and were treated with 10 μL of freshly prepared tetrazolium salt. After 2 h, the plate was assayed at an absorbance wavelength of 450 nm and a reference wavelength of 650 nm (SpectraMax M2e).

### *In vitro* assessment of cell fate after X-ray irradiation.

MDA-MB-231 cells ($10^6$ cells/ml) were incubated for 12 h at 37 °C in 5 % $CO_2$ atmosphere with and without PAuNPs (7.75 μg/mL). The treated cells were washed three times with PBS to eliminate unbound nanoparticles prior to X-ray irradiation. They were exposed to different doses of radiation (2, 4, 6, 8 and 10 Gy; 320 kVp, X-RAD 320) and imaged by fluorescence microscopy to determine their fate. Three hours after X-ray irradiation, the cells were stained with an apoptosis/necrosis kit (ab176749, Abcam, Cambridge, England) at 37 °C and 5 % $CO_2$ for 15 min, then washed three times with PBS. The samples were finally analyzed by fluorescence microscopy using an EVOS FL Cell Imaging System (ThermoFisher Scientific, Santa Clara, CA, USA).

### ROS generation and detection by RPAuNPs in cells.

The fluorescence of cells incubated with either RPAuNPs or PEG-DHR123 (7.75 μg/mL) was assessed to evaluate the formation of ROS in the cell media. MDA-MB-231 cells were cultured and irradiated as described previously. After irradiation, the cells were imaged by fluorescence microscopy (EVOS FL).

### Xenograft mouse model.

MDA-MB-231 cells ($5\times10^6$ cells) were suspended in 50 μL of PBS (pH 7.4, 1X) and injected subcutaneously into the proximal thigh region of male BALB/c-nude mice, 5–8 weeks of age (Charles River, Wilmington, MA). All animal studies were approved and performed according to the guidelines of the Administrative Panel on Laboratory Animal Care (APLAC) at Stanford University, under protocol #31911. Animal welfare was monitored daily both by the researchers and staff veterinarians.

### *In vivo* imaging and evaluation of generated ROS by RPAuNPs.

To image ROS generated *in vivo* by AuNP during X-ray radiation, tumor-bearing mice ($n$=12 mice) were injected intratumorally with either RPAuNPs or PEG-DHR123. Half the

Author Manuscript Author Manuscript Author Manuscript Author Manuscript

mice (3 from each group) were additionally treated using a conformal small-animal irradiation system (X-RAD SmaRT, PXi, North Branford, CT) outfitted with a 1 cm diameter collimator. The other 6 mice did not receive radiation therapy. Radiation treatment planning was performed using RTImage. Cone-beam CT images were acquired prior to radiation therapy to set the radiation isocenter on the center of the tumor. Following radiation therapy, the mice were imaged using the Maestro™ *In-Vivo* Fluorescence Imaging System (Cri Inc., Woburn, MA) with the GFP filter set (excitation: 445490 nm; emission: 515 nm long-pass). The system's tunable liquid-crystal emission filter was configured to acquire 22 spectral images, ranging from 500 nm to 720 nm. Reference spectra were also acquired for mouse skin and RPAuNP green fluorescence, then the images were processed using spectral unmixing to separate the true florescence signal from endogenous autofluorescence.

## 3. Results and Discussion

We synthesized gold nanoparticles (AuNPs) by one-pot synthesis using the reduction protocol [22]. The morphology and size of the particles were efficiently controlled by adjusting the amount of reducing agent. To improve stability and biocompatibility, PEGylated AuNPs (PAuNPs) were prepared by exchanging triton X-100 with heterobifunctional polyethylene glycol (COOH-PEG-SH). The gold-thiol reaction was initiated by the oxidative addition of the S-H bond to the gold, followed by reductive elimination of the hydrogen. The morphology of the prepared AuNPs and PAuNPs was examined by TEM, showing a particle size of 20 nm diameter. Their optical plasmon peaks were analyzed using a UV-vis spectrometer and found a resonance absorption band at 530 nm. We observed that surface modification of the AuNPs solution did not greatly affect their intrinsic morphology and optical properties.

The PAuNPs were further functionalized for sensing radiation-generated ROS near their surface by conjugating them with dihydrorhodamine 123 (DHR-123). DHR-123, the reduced form of rhodamine 123, is a molecular sensor that is nonfluorescent in its initial form but fluorescent after its oxidation by reactive oxygen species (ROS) [23].

Radiation-responsive PAuNPs (RPAuNP) were synthesized by conjugating the carboxylic acid group (-COOH) of the PAuNPs with the primary amine (-NH2) group of DHR123. Nhydrosuccinimide (NHS) was used to allow carbodiimide (EDCs) to form active ester functional groups with carboxylated groups. NHS esters are hydrophilic active groups that react rapidly with the amines of DHR123. Therefore, DHR-123 was covalently bound to the outer ends of the PEG monolayer via carboxylic acid bonds (Scheme 1). TEM images and optical absorption spectra of RPAuNPs were similar to that of AuNPs and PAuNPs (Figure 1, S1). In addition, PAuNPs and RPAuNPs demonstrated excellent colloidal stability in fetal bovine serum (FBS), cell culture media and phosphate-buffered saline (PBS). In contrast, AuNPs showed significant aggregation as they lacked protective PEG chains on their surface (Figure S2).

To validate the feasibility of ROS generation and detection by RPAuNPs, we measured the fluorescence of solutions containing RPAuNPs and DHR123-conjugated PEG (control;

Author Manuscript Author Manuscript Author Manuscript Author Manuscript

referred to as PEG-DHR123), before and after exposure to radiation (2, 4 and 6 Gy; 320 kVp X-ray). For the highest dose (6 Gy), we observed a 7-fold increase in the fluorescence of the RPAuNPs solution but only a 20% increase in the fluorescence of the PEG-DHR123 solution (Figure 2).

We attribute this significant difference to the high concentration of ROS created near the AuNP, as compared to the aqueous solution. In the kV X-ray range, AuNPs have much higher absorption cross-section than water, primarily due to their higher photoelectric absorption. For X-rays in the 100–320 keV energy range (as used on this work), the total stopping power of gold is 50–500 times higher than that of water [24]. X-ray energy absorbed by the NP is transferred to the surrounding molecules by energetic electrons, including photelectrons, Compton recoil electrons, and Auger electrons. These ionizing electrons produce ROS through the radiolysis of water, which then go on to react with DHR-123 located on the NP surface.

We next used a WST-1 assay to determine *in vitro* cytotoxicity of PAuNPs and RPAuNPs in MDA-MB-231 human breast adenocarcinoma cells. Cell viability was examined after incubation with various concentrations of PAuNPs and RPAuNPs for 24 h. As shown in Figure 3, treated MDA-MB-231 cells showed greater than 75 % cell viability at high RPAuNPs concentration (up to 7.75 μg/mL), indicating that PAuNPs and RPAuNPs are biocompatible even at high nanoparticle concentrations.

We also measured the ability of RPAuNPs to enhance radiation damage *in vitro*. We used an apoptosis/necrosis detection kit to evaluate the fate of MDA-MB-231 cells treated with 0–6 Gy X-ray radiation. Three hours after RT, we found that the number of apoptotic cells (green) rose steadily with increasing X-ray radiation dose but necrotic cell death (red) was not observed at the considered timepoint. Importantly, the number of apoptotic cells was larger for cells treated with RPAuNPs (Figure 4a) than for control cells (Figure 4b). This suggests that higher cancer cell killing can be achieved at a lower radiation dose (and, thus, lower normal tissue toxicity).

To verify that enhanced radiation-induced cell killing was mediated by ROS, we measured ROS levels in the immediate vicinity of RPAuNPs by measuring the fluorescence of DHR123 sensor conjugated to the nanoparticle. As previously, MDA-MB-231 cells were treated with PEG-DHR123 (control) and RPAuNPs overnight, then exposed to different doses of X-ray radiation (0–6 Gy). In agreement with our previous measurements in solution, the fluorescence intensity of RPAuNPs increased with increasing radiation dose, whereas the intensity of PEG-DHR123 did not increase significantly (Figure 5a). This finding was verified by quantifying cell fluorescence intensity via ImageJ (Figure 5b and c). Together, these results indicate that high concentrations of ROS are produced near the nanoparticle but not elsewhere, and that these ROS contribute to increased cell death *in vitro*.

Finally, fluorescence imaging was performed to evaluate the feasibility of using RPAuNP to detect, *in vivo*, the generation of ROS near radiation-enhancing gold NPs. Mice bearing MDAMB-231 xenografts were injected with either RPAuNP ($n$ = 6, 15 μg / 100 μL) or PEG-

Author Manuscript Author Manuscript Author Manuscript Author Manuscript

DHR123 ($n$ = 6, 5 mg/ 100 μL). Half the mice in each group ($n$ = 3) further received radiation therapy using a small-animal conformal X-ray irradiator (6 Gy at 225 kVp). On-board cone-beam CT was used to move the radiation isocenter to the center of the tumor. CT imaging also verified the presence in the tumor of the injected nanoparticles (Figure S3). Multispectral fluorescence imaging was used to image fluorescence activation 1 h later (Figure 6a). The images were acquired using the GFP filter set, and the tunable emission filter was configured to scan 22 wavelengths between 500 and 720 nm. Spectral unmixing was applied to separate the green fluorescence of the ROS sensor (shown in green) from skin autofluorescence (shown in red). Significant fluorescent signal (green color) was observed in irradiated tumors but not in control non-irradiated tumors. These findings were confirmed by imaging the excised tumors *ex vivo* (Figure 6b). Furthermore, fluorescence activation was significantly higher in tumors injected with RPAuNPs than in control tumors injected with PEG-DHR123. Quantitative analysis confirmed that, *in vivo*, average photon counts from irradiated RPAuNP tumors were 3–6 fold higher than for controls (Figure 6c). For excised tumors (*ex vivo*), the difference was even wider with 7–14 fold higher fluorescence in irradiated RPAuNP tumors than in control tumors (Figure 6d).

These results indicate that targeted X-ray irradiation of the tumor results in effective formation of ROS near the surface of the gold NP, as we had hypothesized. This effect is primarily mediated by densely ionizing Auger electrons, which are emitted by gold during the radiation treatment, and possibly by the catalytic properties of AuNPs. These results are consistent with previous findings showing that gold nanoparticles sensitize cells to ionizing radiation, especially in the kV range. These nanoparticles may be used as a complement to nanoscale dosimetry simulations, to better understand the physical, chemical and biological effect of AuNP on irradiated cells. In addition, RPAuNPs may serve as a novel theranostic probe for noninvasively monitoring the delivery of conformal radiation therapy in preclinical animal models.

## 4. Conclusion

In summary, we have described the development of a radiation-responsive PEGylated gold nanoparticle (RPAuNPs) and evaluated its ability to monitor ROS levels on its surface during radiation treatment. The rationale for this work is that conventional ROS sensors, which are uniformly distributed, only report average ROS production, ignoring the fact that ROS levels can be orders of magnitude higher in the immediate vicinity of gold nanoparticles. The heterogeneity of ROS levels at the sub-cellular level has significant biological implications. Activation of the fluorescent ROS sensor near the nanoparticle by X-ray radiation was validated *in vivo* using multispectral fluorescence imaging. Potentially, imaging could be performed at greater depth using a near-infrared ROS sensor. To conclude, the advantageous features of this RPAuNP platform could be useful in future research and clinical applications to enhance radiation dose within the tumor and verify the enhanced formation of ROS posttreatment.

## Supplementary Material

Refer to Web version on PubMed Central for supplementary material.

Author Manuscript Author Manuscript Author Manuscript Author Manuscript

## Acknowledgements

This work was performed with support from NIH grants 5R21CA193001 and 1S10OD018208. Guillem Pratx is a Damon Runyon-Rachleff Innovator supported (in part) by the Damon Runyon Cancer Research Foundation (DRR-36–15). Jihye Choi is supported by National Research Foundation (NRF) grants funded by the Korean government, Ministry of Education and Science Technology (NRF-2017M2A2A6A01071157, NRF-2018R1C1B6008799).

## References

[1]. Schaue D and McBride W H 2015 Opportunities and challenges of radiotherapy for treating cancer Nature reviews Clinical oncology 12 527

[2]. Baumann M, Krause M, Overgaard J, Debus J, Bentzen S M, Daartz J, Richter C, Zips D and Bortfeld T 2016 Radiation oncology in the era of precision medicine Nat Rev Cancer 16 234 [PubMed: 27009394]

[3]. Ngwa W, Kumar R, Sridhar S, Korideck H, Zygmanski P, Cormack R A, Berbeco R and Makrigiorgos G M 2014 Targeted radiotherapy with gold nanoparticles: current status and future perspectives Nanomedicine 9 1063–82 [PubMed: 24978464]

[4]. Physics in Medicine and Biology McQuaid HN, Muir MF, Taggart LE, McMahon SJ, Coulter JA, Hyland WB, Jain S, Butterworth KT, Schettino G, Prise KM, Hirst DG, Botchway SW and Currell FJ 2016 Imaging and radiation effects of gold nanoparticles in tumour cells Sci Rep 6 19442 [PubMed: 26787230]

[5]. Hainfeld JF, Slatkin DN and Smilowitz HM 2004 The use of gold nanoparticles to enhance radiotherapy in mice Phys Med Biol 49 N309 [PubMed: 15509078]

[6]. Jain S, Hirst D and O'sullivan J 2012 Gold nanoparticles as novel agents for cancer therapy Br J Radiol 85 101–13 [PubMed: 22010024]

[7]. Carrillo-Cazares A, Jim #xe9, Mancilla-nez NP, Luna-Guti #xe9, rrez MA, Isaac-Oliv #xe9, Camacho-L K #xf3 and pez MA2017 Study of the Optical Properties of Functionalized Gold Nanoparticles in Different Tissues and Their Correlation with the Temperature Increase Journal of Nanomaterials 2017 9

[8]. Mendoza-Nava H, Ferro-Flores G, Ramírez F d M, Ocampo-García B, Santos-Cuevas C, Azorín-Vega E, Jiménez-Mancilla N, Luna-Gutiérrez M and Isaac-Olivé K 2017 Fluorescent, Plasmonic, and Radiotherapeutic Properties of the 177Lu–DendrimerAuNP–Folate–Bombesin Nanoprobe Located Inside Cancer Cells Mol Imag 16 1536012117704768

[9]. Carter J D, Cheng N N, Qu Y, Suarez G D and Guo T 2007 Nanoscale Energy Deposition by X-ray Absorbing Nanostructures The Journal of Physical Chemistry B 111 11622–5 [PubMed: 17854220]

[10]. Ghita M, McMahon SJ, Taggart LE, Butterworth KT, Schettino G and Prise KM 2017 A mechanistic study of gold nanoparticle radiosensitisation using targeted microbeam irradiation Sci Rep 7 44752 [PubMed: 28300190]

[11]. Butterworth KT, McMahon SJ, Currell FJ and Prise KM 2012 Physical basis and biological mechanisms of gold nanoparticle radiosensitization Nanoscale 4 4830–8 [PubMed: 22767423]

[12]. Zheng Y, Hunting D J, Ayotte P and Sanche L 2008 Radiosensitization of DNA by gold nanoparticles irradiated with high-energy electrons Rad Res 169 19–27

[13]. McMahon S J, Hyland W B, Muir M F, Coulter J A, Jain S, Butterworth K T, Schettino G, Dickson G R, Hounsell A R and O'Sullivan J M 2011 Nanodosimetric effects of gold nanoparticles in megavoltage radiation therapy Radiother Oncol 100 412–6 [PubMed: 21924786]

[14]. Kirkby C and Ghasroddashti E 2015 Targeting mitochondria in cancer cells using gold nanoparticle-enhanced radiotherapy: A Monte Carlo study Med Phys 42 1119–28 [PubMed: 25652523]

[15]. Sakata D, Kyriakou I, Okada S, Tran H N, Lampe N, Guatelli S, Bordage M C, Ivanchenko V, Murakami K, Sasaki T, Emfietzoglou D and Incerti S 2018 Geant4-DNA track-structure simulations for gold nanoparticles: The importance of electron discrete models in nanometer volumes Med Phys 45 2230–42 [PubMed: 29480947]

Author Manuscript Author Manuscript Author Manuscript Author Manuscript

[16]. Riley P 1994 Free radicals in biology: oxidative stress and the effects of ionizing radiation International journal of radiation biology 65 27–33 [PubMed: 7905906]

[17]. Lampe N, Karamitros M, Breton V, Brown J M, Kyriakou I, Sakata D, Sarramia D and Incerti S 2018 Mechanistic DNA damage simulations in Geant4-DNA part 1: A parameter study in a simplified geometry Phys Medica 48 135–45

[18]. Nikjoo H, Emfietzoglou D, Liamsuwan T, Taleei R, Liljequist D and Uehara S 2016 Radiation track, DNA damage and response—a review Reports on Progress in Physics 79 116601 [PubMed: 27652826]

[19]. Sicard-Roselli C, Brun E, Gilles M, Baldacchino G, Kelsey C, McQuaid H, Polin C, Wardlow N and Currell F 2014 A new mechanism for hydroxyl radical production in irradiated nanoparticle solutions small 10 3338–46 [PubMed: 24863679]

[20]. Cheng K, Sano M, Jenkins C H, Zhang G, Vernekohl D, Zhao W, Wei C, Zhang Y, Zhang Z and Liu Y 2018 Synergistically Enhancing Therapeutic Effect of Radiation Therapy with Radiation Activatable and Reactive Oxygen Species-Releasing Nanostructures ACS nano

[21]. Su X-Y, Liu P-D, Wu H and Gu N 2014 Enhancement of radiosensitization by metalbased nanoparticles in cancer radiation therapy Cancer Biology & Medicine 11 86–91 [PubMed: 25009750]

[22]. B A J, Markus D and Jessica RF 2015 Simple and Rapid High-Yield Synthesis and Size Sorting of Multibranched Hollow Gold Nanoparticles with Highly Tunable NIR Plasmon Resonances Small 11 4550–9 [PubMed: 26068971]

[23]. Rothe G, Oser A and Valet G 1988 Dihydrorhodamine 123: a new flow cytometric indicator for respiratory burst activity in neutrophil granulocytes Naturwissenschaften 75 354–5 [PubMed: 3211206]

[24]. Berger M J, Hubbell J H, Seltzer S M, Chang J, Coursey J S, Sukumar R, Zucker DS and Olsen KNIST Standard Reference Database 8 (XGAM). ed P NIST, Radiation Physics Division

Author Manuscript Author Manuscript Author Manuscript Author Manuscript

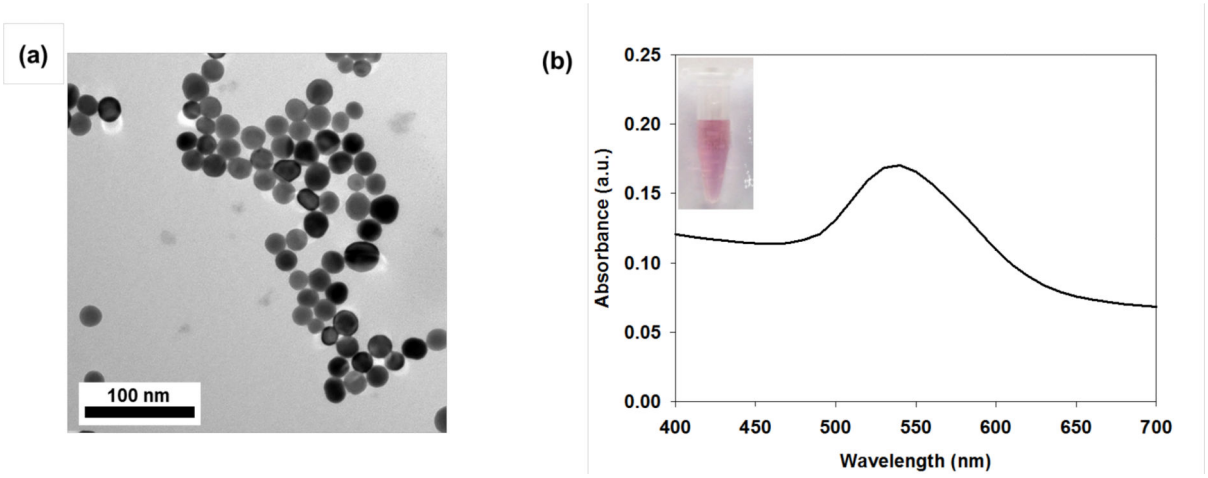


**Figure 1.**

(a) TEM image of RPAuNPs and (b) UV-Vis absorption spectrum of RPAuNPs solution; inset, stability of RPAuNPs in aqueous phase.

Author Manuscript Author Manuscript Author Manuscript Author Manuscript

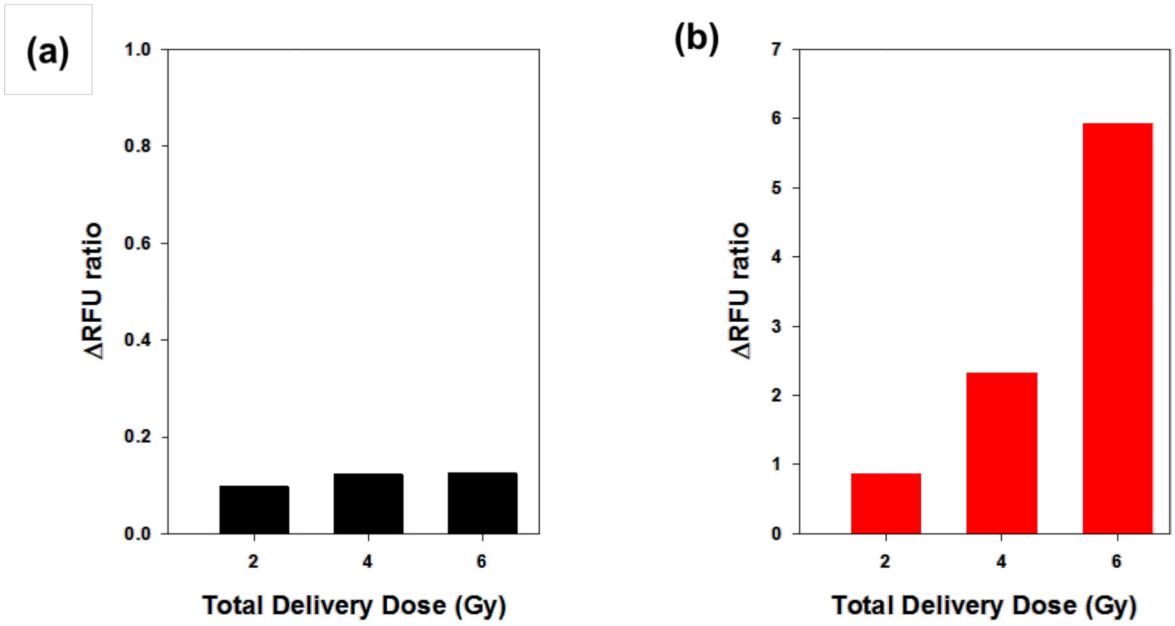


**Figure 2.**

ROS generation and detection in solution. (a) PEG-DHR123 (control) and (b) RPAuNPs, for different doses of radiation (2, 4, and 6 Gy).

Author Manuscript Author Manuscript Author Manuscript Author Manuscript

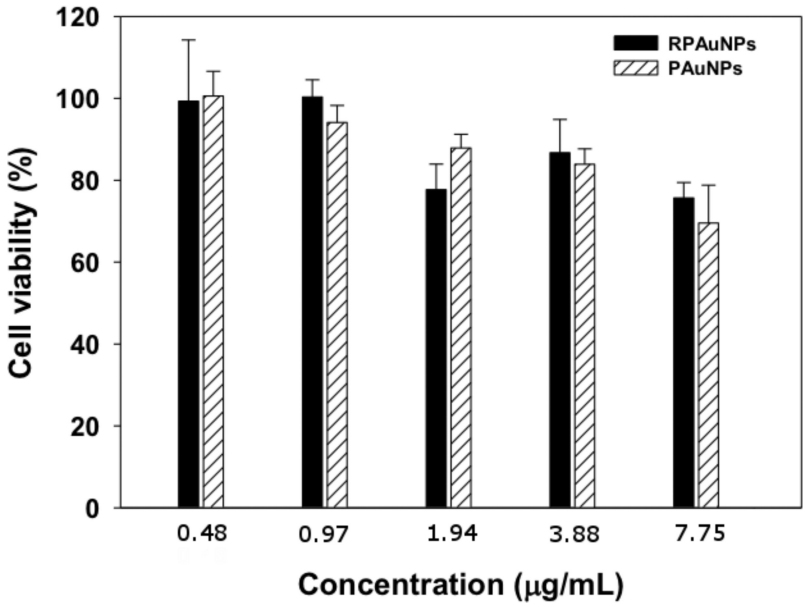


**Figure 3.**
Growth-inhibition of MDA-MB-231 cells treated with PAuNPs and RPAuNPs, measured using WST-1 assay.

Author Manuscript Author Manuscript Author Manuscript Author Manuscript

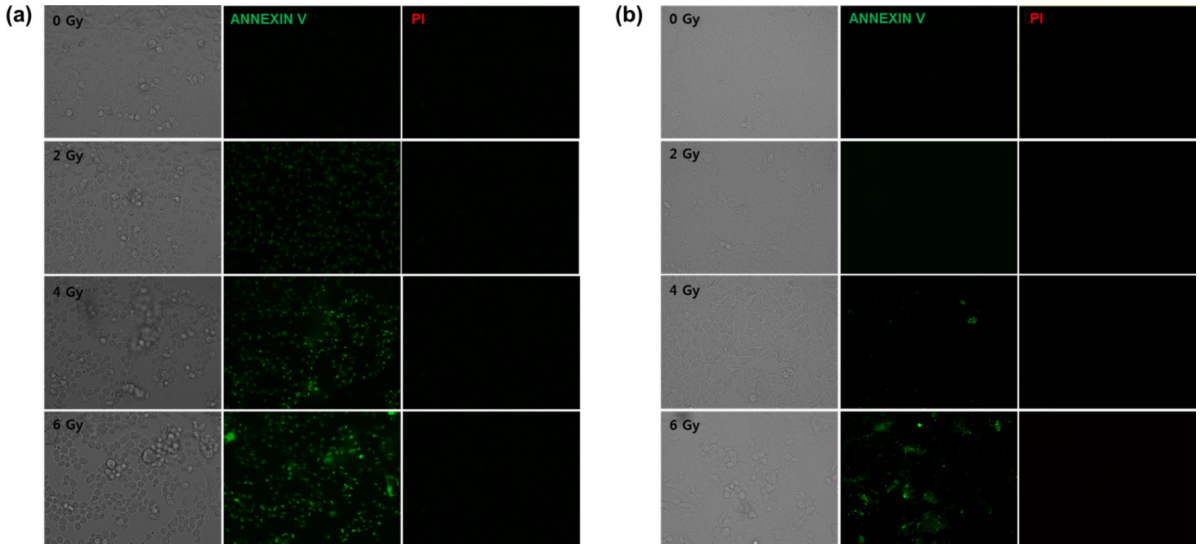


**Figure 4.**

Apoptosis and necrosis in MDA-MB-231 cells following exposure to X-ray radiation. (a) Cells incubated with PAuNPs (b) control cells without nanoparticles.

Author Manuscript Author Manuscript Author Manuscript Author Manuscript

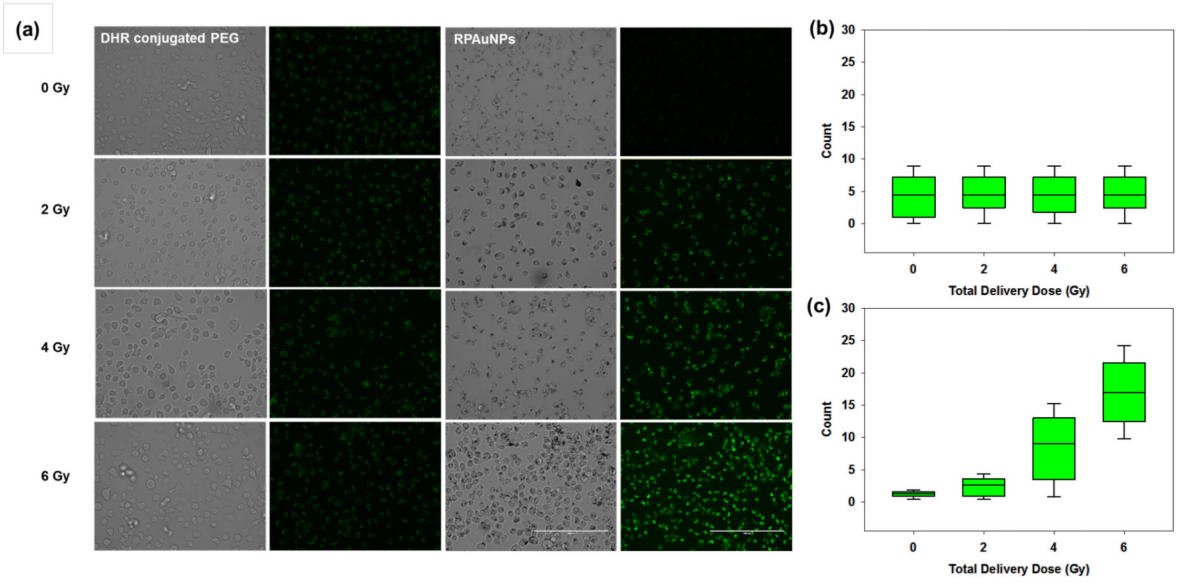


**Figure 5.**

ROS generation measured by imaging DHR-123 fluorescence in irradiated MDAMB-231 cells. (a) Fluorescence microscopy images for cells incubated with PEG-DHR123 (control) or RPAuNPs. (b,c) Quantification of the fluorescence images for cells incubated with PEG-DHR123 or RPAuNPs, respectively.

Author Manuscript Author Manuscript Author Manuscript Author Manuscript

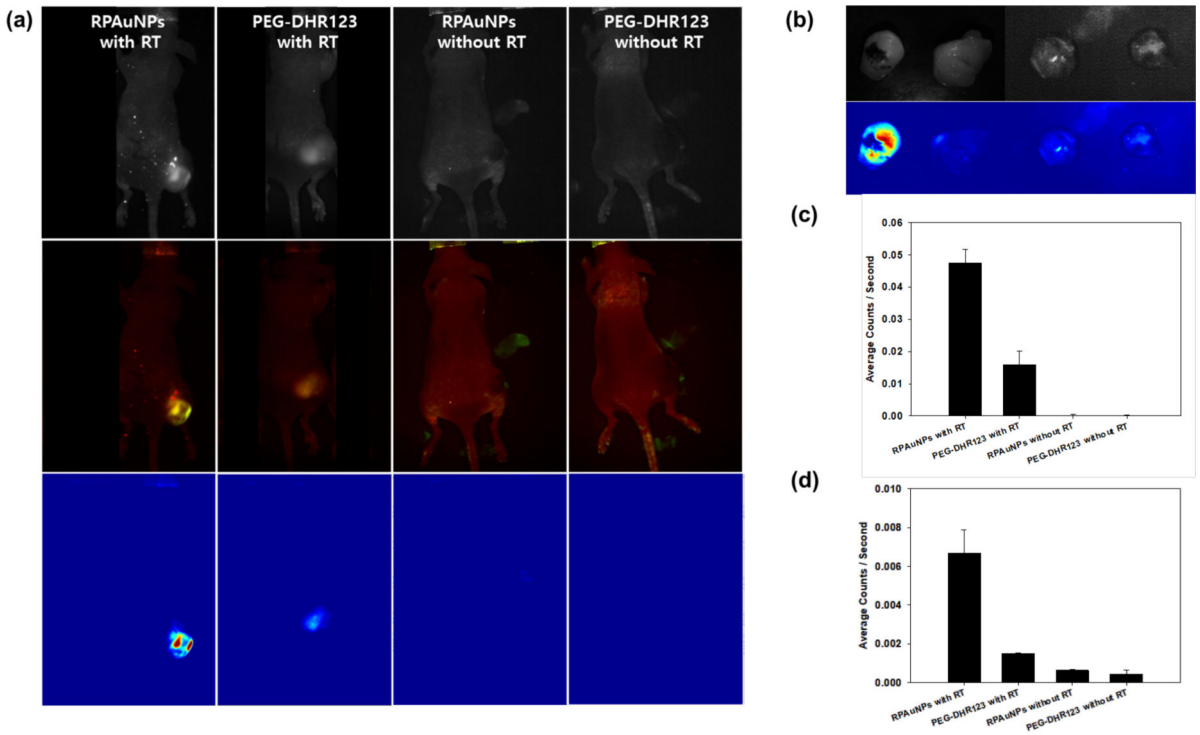


**Figure 6.**

ROS generation and detection in vivo using RPAuNPs. (a, *top row*) Raw *in vivo* fluorescence images acquired with the tunable emission filter set to 530 nm, for mice injected wither either RPAuNPs or PEG-DHR123, and either exposed to 6 Gy RT or no RT. (a, *middle row*) Two-component images showing DHR123 fluorescence (green) and skin autofluorescence (red), obtained by spectral unmixing. (a, *bottom row*) DHR123 fluorescence, obtained by spectral unmixing. (b) Same tumors, imaged *ex vivo*, showing reflectance image (top) and unmixed fluorescence image for the DHR123 component (bottom). (c) Fluorescence counts obtained from unmixed DHR123 *in vivo* images. (d) Same as previous, for *ex vivo* images.

Author Manuscript Author Manuscript Author Manuscript Author Manuscript

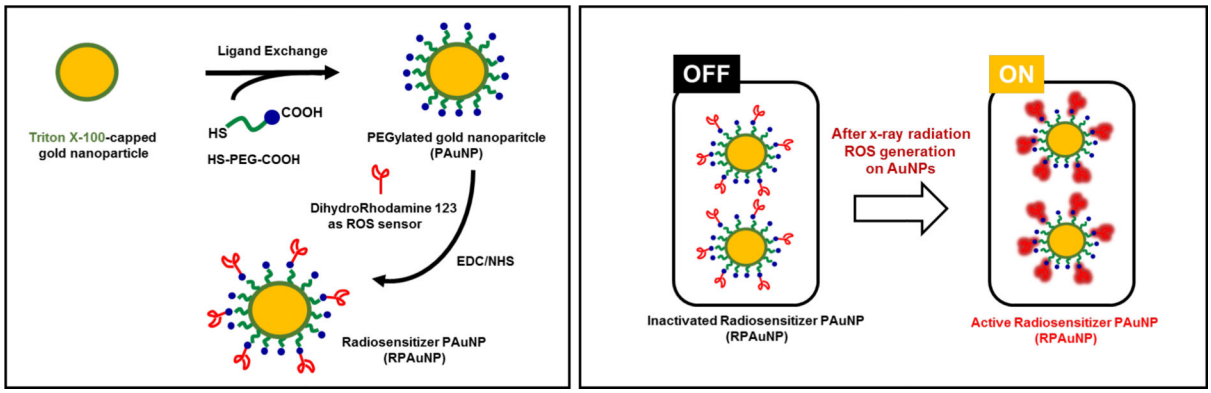


**Scheme 1.**

Schematic illustration showing synthesis of radiation-responsive PEGylated goldnanoparticles (RPAuNP) for ROS generation and detection in cancer radiotherapy.